

Zero-noise Extrapolation Assisted with Purity for Quantum Error Mitigation

Tian-Ren Jin,^{1,2} Zheng-An Wang,^{3,4} Tian-Ming Li,^{1,2} Kai Xu,^{1,2,3,4,5,6,*} and Heng Fan^{1,2,3,4,5,6,†}

¹*Institute of Physics, Chinese Academy of Sciences, Beijing 100190, China*

²*School of Physical Sciences, University of Chinese Academy of Sciences, Beijing 100049, China*

³*Beijing Academy of Quantum Information Sciences, Beijing 100193, China*

⁴*Hefei National Laboratory, Hefei 230088, China*

⁵*Songshan Lake Materials Laboratory, Dongguan 523808, China*

⁶*CAS Center for Excellence in Topological Quantum Computation, UCAS, Beijing 100190, China*

Quantum error mitigation is the technique to post-process error occurring in the quantum system, which reduces the expected errors to achieve higher accuracy. Zero-noise extrapolation is one of the methods of quantum error mitigation, which first amplifies the noise and then extrapolates the observable expectation of interest reversely to the noise-free point. Conventionally, this method depends on the error model of noise, since error rates for degree of noise are presumed in the procedure of noise amplification. In this paper, we show that the purity of output states of noisy circuits can assist in the extrapolation procedure to avoid the presumption of error rates. We also discuss the form of fitting model used in extrapolation. We verify this method and compare it with the ordinary zero-noise extrapolation method via numerical simulations and experiments on the cloud-based quantum computer, *Quafu*. It is shown that with the assistance of purity, the extrapolation is more stable under the random fluctuation of measurements and different kinds of noise.

I. INTRODUCTION

It is believed that quantum computation should have superiority beyond the classical computation for certain problems. However, the realization of a useful quantum computer is difficult because the qubits are vulnerable to the noise of environment. Thus, fault-tolerant quantum computation is vital to the application of quantum computation. Quantum error correction code (QECC) provides a systematic solution to fault-tolerant quantum computation [1], while whose application requires many physical qubits and error rate should be lower than a threshold [2–4]. With remarkable progresses [5, 6], however, it is challenging for the state-of-the-art technique to meet the requirements for the full implementation of QECCs. Therefore, the fault-tolerant quantum computation based on high precision logic qubits is still a far-reaching task.

In the noisy intermediate-scale quantum era [7], quantum error mitigation (QEM) provides an alternative technique for noise processing. QECCs detect and correct the errors occurring in the quantum process to make sure that there is no error occurring on coded logic qubits. On the contrary, QEMs allow the occurring of error, but use some post-processing techniques to reduce the bias between the output information of noisy quantum circuit and the ideal quantum circuit [8–10].

In recent years, several QEM schemes are proposed, like zero-noise extrapolation (ZNE) [11–14], probabilistic error cancellation (PEC) [12, 13], symmetry verification methods [15–17], purification methods [18–21], and subspace expansion [22]. These methods have been applied in different quantum computation platforms and different problems [23–36]. Besides, there are efforts to unify the different QEM schemes in some generalized frameworks [10, 17, 37, 38]. The symmetry verification, subspace expansion, and purification methods

are the post-processing methods of quantum state, and have been tried to unify in one framework [37]. The ZNE and PEC methods deal with the quantum circuit, thus relate to the error model of noise. The PEC method mitigates the error by post-cancelling the noise, which is previously estimated from experiments in selected error basis. Thus, the effectiveness of PEC closely depends on the error model described by the error basis. Recently, there is attempt to incorporate ZNE into the PEC framework [38].

However, the case of the ZNE method is subtle. This method is based on the analyticity of the observable expectation with respect to the error rate, which is a general physical condition. The relation to error model is emerged when error rate is considered. To perform the ZNE, the error should be amplified, and the ideal value is obtained by extrapolating the expectation reversely to the point of zero noise. In the early application, the error is amplified by stretching the time of pulse for each gate [23], and they have to verify that the error is time scalable. This amplification is not suitable for digital quantum gate also. Other implementation is by deliberately adding redundant gates in circuit [24]. Then, a treatment called unitary folding is put forward [39]. In this method, the circuit is evolved forward and backward successively, and the error rate is characterized by the number of folding. Although, the amplifications of the error are developed more feasible, the estimation of error rate is *a priori*, which has limitation on the noise type. Moreover, for the complex circuit in experiment, the effect of errors can hardly be parametrized only by a single parameter of error rate.

The universality of the basic idea of the ZNE method is different from the dependency of error rate on the noise type in implementation. In this paper, we try to release the limitation of noise in the ZNE method, by determining the error rate posteriorly from experiment. We propose that purity can be used to determine the error rate. Moreover, we can perform the extrapolation on the measured purity, instead of the presumed error rate.

This paper is organized as follows. In Sec. II, we review the

* kaixu@iphy.ac.cn

† hfan@iphy.ac.cn

ordinary ZNE method, and analyze how this method is based on the error model of noise. Then, we show that the purity of output state can assist the extrapolation in zero-noise error mitigation in Sec. III. We describe the details of extrapolation with purity in Sec. IV, including the form of fitting model, purity estimation methods, and the measurement overhead. We also verify this method by numerical simulations and experiments on *Quafu* cloud-based quantum computer in Sec. V. The conclusion and discussion are given in Sec. VI.

II. ZERO-NOISE EXTRAPOLATION WITH UNITARY FOLDING

The ZNE method consists of two steps:

1. **Noise amplification:** Collecting the raw data of different error rates via measuring on modulated circuits.
2. **Extrapolation:** Post-processing the experiment data to obtain the mitigated expectation value based on some fitting models.

In this section, we will review the ZNE method, the fitting models, and the noise amplification method of unitary folding. Besides, we discuss how the presumption that error rate is proportional to the number of folding is based on the error model of noise.

Let the ideal unitary circuit of interest be \mathcal{U} . In practice, we cannot perform this circuit exactly, but a noisy one \mathcal{U}_λ instead. Then the experimental expectation value $\langle \hat{O} \rangle_\lambda = \text{Tr}[\hat{O}\rho_\lambda]$ of observable \hat{O} of interest is different from the ideal one $\langle \hat{O} \rangle_0 = \text{Tr}[\hat{O}\rho_0]$, where $\rho_\lambda = \mathcal{U}_\lambda(\rho)$ is the noisy output state, and $\rho_0 = \mathcal{U}(\rho)$ is the ideal output state. Now, we are going to infer the ideal value $\langle \hat{O} \rangle_0$ from some noisy expectation values $\langle \hat{O} \rangle_\lambda$.

This method is inspired by a simple idea that the expectation value $\langle \hat{O} \rangle_\lambda$ is an analytic function of a parameter $\lambda \geq 0$, which characterizes the volume of noise of noisy circuit \mathcal{U}_λ , and assume $\langle \hat{O} \rangle_\lambda = \langle \hat{O} \rangle_0$ when $\lambda = 0$. With the definition of analyticity, the expectation value can be expanded in a power series of λ as

$$\langle \hat{O} \rangle_\lambda = O(\lambda) = \sum_{n=0}^{\infty} O_n \lambda^n, \quad (1)$$

and by definition of λ , we have $O_0 = O(0) = \langle \hat{O} \rangle_0$. So by interpolation the function $O(\lambda)$ with expectations $\langle \hat{O} \rangle_{\lambda_i}$ of different error rate λ_i , one can infer the noise-free expectation value $\langle \hat{O} \rangle_0$.

For the number of experimental data is finite, the expansion of $O(\lambda)$ should be truncated at some order M of λ , which requires that the error rate λ should small enough, and this is the polynomial model of function $O(\lambda)$ [11, 12]. Besides, there are also (multi-)exponential model [14]

$$\langle \hat{O} \rangle_\lambda = O(\lambda) = \sum_{a=0}^M B_a e^{-\gamma_a \lambda}, \quad (2)$$

and poly-exponential model [39]

$$\langle \hat{O} \rangle_\lambda = O(\lambda) = e^{f(\lambda)} + O_\infty, \quad (3)$$

where $f(\lambda)$ is a polynomial of λ . These fitting model are put forward under the consideration that the physical observable should be bounded.

Then, the noisy data of different error rate λ_i is obtained by error amplification. The unitary folding performs the circuit sequence in experiment

$$\mathcal{U}_n = \mathcal{U}_\lambda \circ (\mathcal{U}_\lambda^\dagger \circ \mathcal{U}_\lambda)^n = (\mathcal{U}_\lambda \circ \mathcal{U}_\lambda^\dagger)^n \circ \mathcal{U}_\lambda, \quad (4)$$

where the corresponding error rate is expected as $\lambda_n = (2n+1)\lambda_0$, and the resolution is $2\lambda_0$. To have a more fine-grained resolution, it can also perform the layer (gate) folding [39], which assumes the gate can be decomposed into layers $\mathcal{U}_\lambda = \prod_{i=1}^d \circ \mathcal{L}_i$, and performs the folding on these layers

$$\mathcal{L}_i \mapsto (\mathcal{L}_i \circ \mathcal{L}_i^\dagger)^n \circ \mathcal{L}_i \quad (5)$$

in the circuit. By doing so, the resolution can be promoted to $2\lambda/d$.

To consider the procedure of unitary folding in more detail, we assume the circuit is a gate only, and set the noisy in forward and backward evolutions as

$$\mathcal{U}_\lambda = \mathcal{E}_f \circ \mathcal{U}, \quad (6)$$

$$\mathcal{U}_\lambda^\dagger = \mathcal{U}^\dagger \circ \mathcal{E}_b, \quad (7)$$

which can be interpreted as the definition of the forward error \mathcal{E}_f and backward error \mathcal{E}_b , whose error rate is denoted as λ_f and λ_b correspondingly. Then, we formally have

$$\mathcal{U}_\lambda \circ \mathcal{U}_\lambda^\dagger = \mathcal{E}_f \circ \mathcal{E}_b \equiv \mathcal{E}, \quad (8)$$

thus the noisy gate is

$$\mathcal{U}_n = \mathcal{E}_n \circ \mathcal{U}, \quad (9)$$

where $\mathcal{E}_n = \mathcal{E}^n \circ \mathcal{E}_f$ is the error channel with the error rate $\lambda_n = n\tilde{\lambda} + \lambda_f$, where $\tilde{\lambda}$ is the error rate of error channel \mathcal{E} .

To obtain $\lambda_n = (2n+1)\lambda_f$, we should assume $\tilde{\lambda} = 2\lambda_f$, which is true when the error channel satisfies $\mathcal{E}_f = \mathcal{E}_b$. However, this assumption is not always realized, if we approximate $\tilde{\lambda} \approx 2\lambda_f$, it will introduce additional error in the inference of the ideal value $O(0)$ before fitting the data of experiments. Thus, the ZNE method constrained by the error model of noise. The simplest way to solve this problem is to determine the error rate λ from experiments.

III. EXTRAPOLATION WITH PURITY

Fidelity is always used to witness the difference between the state with an ideal state, however the ideal state ρ_0 cannot be prepared precisely for the unavoidable noise in experiment. Thus, to measure the fidelity of noisy state and ideal state re-

quires the classical simulation of the quantum circuit, which is not feasible in general for large system. In this section, we will describe the idea of using the purity of the output state of noisy circuit

$$p(\rho_\lambda) = \text{Tr}|\rho_\lambda|^2 = \text{Tr}(\rho_\lambda^\dagger \rho_\lambda) \quad (10)$$

to reflect the influence of noise in circuit. The ideal unitary circuit will not influence the purity of state. We assume the error is not unitary, otherwise it can be cancelled by the folding of well calibrated circuit. Then, the influence of noise on the observable expectation is reflected by the influence on the purity.

In the unitary folding, the folded channel, which is denoted as χ here, defines a homogenous linear difference equation

$$\rho(x+1) = \chi(\rho(x)), \quad (11)$$

in the matrix space, where x is a continuous variable of the folding number n , which is proportional to the error rate λ , and we call x also as error rate in the following. Therefore, the phase flow of this equation $g^x : \rho(0) \mapsto g^x \rho(0) = \rho(x)$, is determined by the channel χ completely. The extrapolation is actually to infer the ideal expectation along the phase flow where the ideal output state $\rho(0)$ located.

For the error amplification procedure via unitary folding, we consider the following two folding sequences

$$\tilde{\mathcal{U}}_n = (\mathcal{U}_\lambda^\dagger \circ \mathcal{U}_\lambda)^n, \quad (12)$$

$$\mathcal{U}_n = (\mathcal{U}_\lambda \circ \mathcal{U}_\lambda^\dagger)^n \circ \mathcal{U}_\lambda. \quad (13)$$

There are two different folded channels $\mathcal{U}_\lambda^\dagger \circ \mathcal{U}_\lambda$, $\mathcal{U}_\lambda \circ \mathcal{U}_\lambda^\dagger$, which correspond to two different phase flows. In the folding sequence of $\tilde{\mathcal{U}}_n$, noise-free state is located at $n = 0$, but this sequence contains no information of ideal evolution \mathcal{U} . Therefore, we should extrapolate the expectation following this sequence to the noise-free point, but the expectations cannot be measured from this sequence. In the contrary, the folding sequence \mathcal{U}_n contains the information of ideal channel \mathcal{U} , while the noise-free point is not located in its phase flow. Although we can obtain the expectations of observable, we cannot extrapolate to the noise-free point following this sequence.

The purity of output state can connect the phase flows of the two folding sequences. With the forward and backward errors defined above, we have

$$\mathcal{U}_n = \mathcal{E}_n \circ \mathcal{U}, \quad (14)$$

$$\tilde{\mathcal{U}}_n = \mathcal{U}^\dagger \circ \tilde{\mathcal{E}}_n \circ \mathcal{U}, \quad (15)$$

where

$$\mathcal{E}_n = (\mathcal{E}_f \circ \mathcal{E}_b)^n \circ \mathcal{E}_f, \quad (16)$$

$$\tilde{\mathcal{E}}_n = \mathcal{E}_b \circ \mathcal{E}_{n-1} = (\mathcal{E}_b \circ \mathcal{E}_f)^n. \quad (17)$$

Now, we consider another sequence

$$\check{\mathcal{U}}_n = \tilde{\mathcal{E}}_n \circ \mathcal{U}, \quad (18)$$

where the noise-free point is located, and the information of forward circuit \mathcal{U} is maintained. This sequence is the one suitable for our extrapolation, but cannot be performed via the unitary folding technique. However, the purity of the output state of this circuit sequence

$$p(\check{\mathcal{U}}_n(\rho)) = p(\tilde{\mathcal{U}}_n(\rho)) \quad (19)$$

is same as the sequence $\tilde{\mathcal{U}}_n$, for purity is invariant under unitary evolution. This allowed us to label the phase flow of $\tilde{\mathcal{U}}_n(\rho)$ with purity measured from experiment. The error rate of $\tilde{\mathcal{U}}_n$ is $x = n$ without problem when $x = 0$ denotes the noise-free point, and purity of output state of $\tilde{\mathcal{U}}_n$ allows us find the function $p(x)$ on the phase flow of the sequence $\tilde{\mathcal{U}}_n$. Then, the error rate x_n of \mathcal{U}_n should satisfy

$$p(x_n) = p(\mathcal{U}_n(\rho)), \quad (20)$$

where the purity $p(\mathcal{U}_n(\rho))$ can be measured from experiments. Particularly, the difference $\lambda_n = x_n - x_{n-1}$ of error rate should not be uniform for different n in general. With the value of x_n , we can fit the curve of expectation $O(x)$ versus error rate x with the experimental data $O(x_n) = \text{Tr}(\hat{O}\mathcal{U}_n(\rho))$ to the noise-free point $x = 0$.

However, solving the error rate x_n from purity is not an easy task. We can extrapolate to the noise free point direct on the purity instead. To do so, we measure the purity $p(0)$ of the noise-free state from the circuit $\tilde{\mathcal{U}}_0$ without evolution \mathcal{U}_λ . This purity $p(0)$ describe the error occurring in the procedure of preparation and measurement, which cannot be amplified by unitary folding. Here, we should assume the noise of preparation and measurement is mitigated beforehand. The reason we measure the noise-free state purity $p(0)$ is that we cannot always assume the initial state is always a pure state. However, if the ideal state is pure state, we can assume $p(0) = 1$, and the above procedure can be interpreted as a way to “purify” the noisy state. Different with the QEM method of purification, which virtually purifies a mixed state to the pure state closest to it, here the noisy state is virtually purified along the phase flow of the noise.

IV. DETAILS OF METHODS

In Sec. III, we discuss how purity can help the extrapolation. However, it is necessary to describe it in detail for its application. The accuracy of extrapolation depends on the fitting model. What should be the suitable form of fitting model? Different with ordinary ZNE method, we should measure the purity in addition to determine the error rate here. How to estimate the purity in experiments? In this section, we will discuss the reasonable fitting models, and introduce the method can be used to estimate purity. Besides, we will discuss the overhead of measurement of this mitigation method.

A. Fitting Model

With the assumption of the analyticity of the expectation $O(x)$ with respect to the error rate x , we can expand it into a power series. However, the experiment data are finite, thus it should be truncated as a polynomial. This model is not perfect, since it is in effect only when the error rate is small enough. Moreover, when error rate $x \rightarrow \infty$, the polynomial fitting model will give divergence also. But, the state $\rho(\infty)$ is still normalized, thus $O(\infty) = \text{Tr}[\hat{O}\rho(\infty)] \leq \|\hat{O}\|_\infty$, where $\|\hat{O}\|_\infty$ is the spectrum radius, the supremum of moduli of eigenvalues, of the observable \hat{O} . The spectrum radius of the observable \hat{O} of finite dimension quantum system, qubits or qudits, are always finite. Even in the continuous quantum system, which allows the infinity spectrum radius, the infinity is not a real experience, but a limit. Thus, the boundedness of physical observable is convinced. The simplest fitting model, exponential model, with the additional assumption of boundedness is proposed, and then the multi-exponential model and the poly-exponential model.

Although all these models are reasonable, we can derive the fitting model in more detail. Here, we notice that all the quantum channels (without post selection) are linear, which give a homogenous linear difference equation, Eq (11). With this property, we conclude from the theory of linear differential equation that the solutions are linear combination of quasi-polynomials $q_k(x) = P_k(x)e^{kx}$, where $P_k(x)$ are polynomials. Then, we show the details.

In an orthonormal basis $|i\rangle$, we choose the matrix basis $M_i^j \equiv |i\rangle\langle j|$, with the multiplication rule $M_i^j M_k^l = \delta_k^j M_i^l$. With this basis, we expand the super-operators χ as

$$\chi(\rho) = \chi_{j|i}^i M_i^j \rho M_k^l, \quad (21)$$

and density matrix

$$\rho = \rho_n^m M_m^n. \quad (22)$$

Here we adopt the Einstein convention that repeated index means summation. By simple calculation, we get the tensor representation of super-operator on operators

$$\chi(\rho)_j^i = \chi_{m|j}^i \rho_m^m. \quad (23)$$

It is possible to rephrase this representation in the more familiar form of vector [40], which just raises the “bra” index of the density matrix, thus we are still working in the tensor here.

We now consider the phase flow defined by a channel χ in the matrix space

$$\rho_j^i(x+1) = \chi_{m|j}^i \rho_m^m(x), \quad (24)$$

where $\chi_{m|j}^i$ is the tensor of channel χ . There exist a “unitary” transformation u , which preserve the inner product $(\hat{A}, \hat{B}) = \text{Tr}(\hat{A}^\dagger \hat{B})$ of matrix space, transform the tensor χ into Jordan canonical form, in some orthonormal matrix basis. This transformation preserve the Frobenius norm of density matrix, namely the square root of purity $p(\rho)$, but not the trace, thus

may be non-physical. Notice that the unitary transformation is performed on density matrix ρ_n^m , which only preserve the norm of purity $p(\rho)$ of density, but not the trace, thus may not be physical. Under this transformation, the density ρ_j^i is transformed into a non-normalized “state” $\tilde{\rho}_j^i$, which is the root vector of χ , thus has the form of quasi-polynomial

$$\tilde{\rho}_j^i(x) = \tilde{\chi}_{ij}^x P_{ij}(x), \quad (25)$$

where $\tilde{\chi}_{ij}$ are the eigenvalues of χ , and $P_{ij}(x)$ are polynomials whose degree are less than the order of corresponding eigenvalues $\text{ord}\tilde{\chi}_{ij}$. Since it is possible that some eigenvalues are same, we reorder them as $\tilde{\chi}_a$, where a runs from 0 to M , and in original basis the density matrix is linear combination of these quasi-polynomials

$$\rho_j^i(x) = \sum_a P_{aj}^i(x) \tilde{\chi}_a^n. \quad (26)$$

On the other hand, because the unitary transformation u preserves the norm of purity, thus the purity is also the linear combination of quasi-polynomials

$$p(\chi^n(\rho)) = p(\tilde{\chi}^n(\tilde{\rho})) = \sum_a A_a(x) |\tilde{\chi}_a|^{2n}, \quad (27)$$

where $\deg A_a < 2\text{ord}\tilde{\chi}_a$. Since the purity is over the bounded range $[1/d, 1]$, $|\tilde{\chi}_a| \leq 1$ must be satisfied. Defining k_a satisfying $e^{-k_a} = \tilde{\chi}_a$, we get the quasi-polynomials model of observable and purity

$$O(x) = \sum_{a=1}^M B_a(x) e^{-k_a x} + B_0, \quad (28)$$

$$p(x) = \sum_{a=1}^M A_a(x) e^{-2\Re(k_a)x} + A_0, \quad (29)$$

where $k_0 = 0$, $B_a = O_i^j P_{aj}^i$, and O_i^j is the matrix element of operator \hat{O} . The reason that the polynomials A_0, B_0 has zero degree is that otherwise they will be divergent at infinity. In the large error limit $x \rightarrow \infty$, the state can be set as the maximal mixed state I/d , thus $A_0 = 1/d$, $B_0 = \text{Tr}\hat{O}/d$, or we can fit A_0, B_0 from experiment data.

Now we can fit the curve on experiment data with this quasi-polynomial form as mentioned before. However, the number of eigenvalues and the degree of corresponding quasi-polynomials depend on the specific error, which is unknown, thus we must perform some approximation in practice. For example, we may assume the degree of quasi-polynomials corresponding to each eigenvalue are all the same, then the number of eigenvalues should be determined by the size of experiment data. For more simplicity, the degree of quasi-polynomials may be assigned as zero, which reduce to the multi-exponential model. Moreover, by view the n -th degree coefficients of polynomial with different exponential decay as non-normalized quasi-probabilistic measures of index a , by

cumulant expansion, the model can be written as

$$O(x) = \sum_n x^n e^{-v_n(x)} + B_0, \quad (30)$$

$$p(x) = \sum_n x^n e^{-u_n(x)} + A_0, \quad (31)$$

where the coefficients of polynomials $u_n(x), v_n(x)$ are the cumulants of k_a . With the approximation that the degree of quasi-polynomials is zero, this model is reduced to the poly-exponential model. Besides, if we assume the decay rate k_a of exponential function is zero, we come back to polynomial model. Thus, the quasi-polynomial model from linearity of quantum channel allows us to unify all the fitting models have been proposed.

As previously mentioned, we can fit the expectation versus the purity, but the rigid form of fitting model will be more complex and cannot be explicitly written out here. However, we can write a phenomenological fitting model at here. We represent the purity p as an index $s = \ln \frac{d-1}{dp-1}$, where d is the dimension of system, so this index s equal to 0 at pure state, and ∞ at maximal mixed state. So, this index is an error-rate-like index, with which we can temporarily write the fitting model as the form of quasi-polynomial by substituting the error rate x . For s is not the real error rate, we must generalize the quasi-polynomial model, which can be taken as the form of “quasi-poly-exponential”

$$O(s) = \sum_j g_j(x) e^{-f_j(s)} + B_0, \quad (32)$$

where $f_j(s), g_j(s)$ are some polynomials of s . This model can also be reduced to the case of multi-exponential or poly-exponential form as the approximations having used.

B. Purity Evaluation

In this subsection, we will introduce the purity measurement method. Since purity is not a linear operator of density matrix, thus it cannot be easily evaluated in experiments. The most trivial way to measure the purity is to perform the quantum state tomography (QST), and then calculate the purity by definition. However, QST is so expensive that it is hard to perform on a large system. This difficulty may hinder the usage of purity in extrapolation. We can reduce the size of system we measured. If the operator we care about is located on some sites, we can only measure the purity of these sites. Nevertheless, there may exist the case we must measure the purity of a relatively large system. Therefore, we need more efficient methods to measure the purity.

The purity can be measured by random measurement [41], where we randomly measure the operators sampled from an ensemble, typically the Pauli string of the qubits. The circuit is shown in Fig. 1. This method is called classical shadow, which can substitute QST. By random measurement of operators with the Monte Carlo sampling, this method is more efficient than QST for large size system. The number of mea-

surements is shown as the order of

$$\sim \frac{\log(M) \sup_i \|O_i\|}{\epsilon^2}, \quad (33)$$

which is determined by the observable operators $\hat{O}_i, (i = 1, \dots, M)$ of interest, the ensemble of unitary gates, and the precision ϵ .

In purification method, the measurement of quantities $\text{Tr}(\rho^M)$ are key problem. The measurement method with replica is proposed, which is founded on the following equation

$$\text{Tr}(\hat{O}\rho^M) = \text{Tr}(\hat{O}_{(i)}\hat{S}^{(M)}\rho^{\otimes M}), \quad (34)$$

where $\rho^{\otimes M}$ is M copies of ρ , $\hat{O}_{(i)}$ is the operator \hat{O} acted on the i -th copy, typically $i = 1$, and $\hat{S}^{(M)}$ is cyclic permutation on M copies

$$\hat{S}^{(M)} |\psi_1\rangle \otimes |\psi_2\rangle \otimes \dots \otimes |\psi_M\rangle = |\psi_2\rangle \otimes \dots \otimes |\psi_M\rangle \otimes |\psi_1\rangle. \quad (35)$$

The purity can be mapped to the expectation of $\hat{S}^{(2)}$ on two-replica state $\rho^{\otimes 2}$. The circuit of $\hat{S}^{(M)}$ is shown in Fig. 2. This method allows us to measure the purity directly from the quantum circuit, which is generally used in the so-called virtual distillation or error suppression by derangement (VD/ESD) in the purification method [19]. Although it can reduce the exponentially increasing of quantities measured in QST, it enlarges the space complexity of qubits for the preparation of 2 copies, and the SWAP gates needed in applying $\hat{S}^{(2)}$ will enlarge the time complexity of quantum circuit.

C. Extrapolation with Echo

Beside the above-mentioned methods in last subsection, there is a variation of purity estimation called echo or state verification. Inspired by this echo protocol of purification method [17], we modify the extrapolation method. We consider the purity of $\rho(x) = \mathcal{U}_x(\rho)$, where \mathcal{U}_x is $2x + 1$ folds of

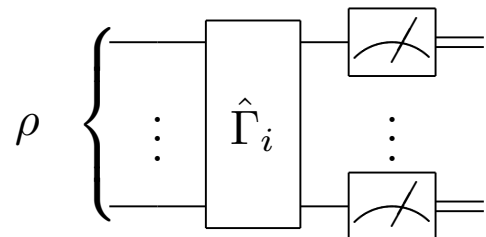
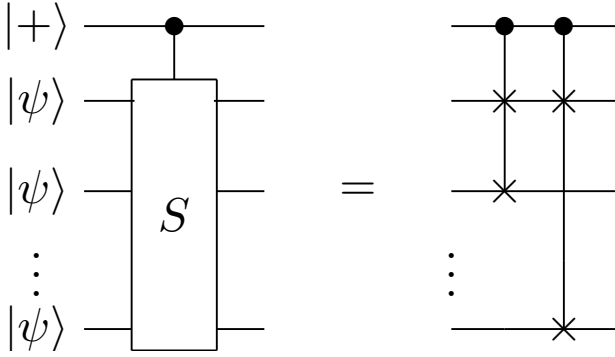


FIG. 1. The circuit of random measurement. The gate $\hat{\Gamma}_i$ is uniformly sampled from an ensemble of unitary gates, like the n -qubit or tensor products of single-qubit Clifford unitaries. The quantum state ρ can be recovered from the n -bit measurement outcome and the choice of the unitary gate $\hat{\Gamma}_i$

FIG. 2. The circuit of $\hat{S}^{(M)}$.

\mathcal{U}_λ , then the purity of the output state

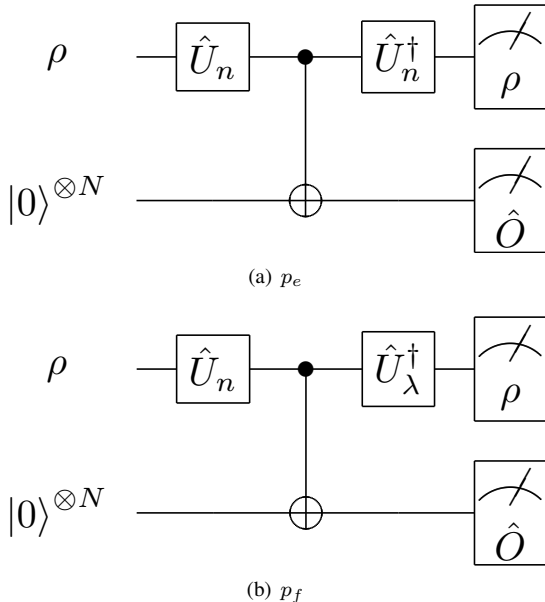
$$\begin{aligned} p(x) &= \text{Tr} \rho(x)^2 = \text{Tr} [\mathcal{U}_x(\rho)^2] \\ &= \text{Tr} [\rho (\mathcal{U}_x)^\dagger \circ \mathcal{U}_x(\rho)] = \text{Tr} [\rho \hat{\rho}_x], \end{aligned} \quad (36)$$

is the overlap of initial state ρ with quasi-state $\hat{\rho}_x = (\mathcal{U}_x)^\dagger \circ \mathcal{U}_x(\rho)$, which is not physical in general. Here, the \dagger on the channel \mathcal{U}_x is acted on its Kraus operators, but not the output state $\mathcal{U}_x(\rho)$. For $\mathcal{U}_x = (\mathcal{U}_\lambda \circ \mathcal{U}_\lambda^\dagger)^n \circ \mathcal{U}_\lambda$, the quasi-channel is

$$(\mathcal{U}_x)^\dagger \circ \mathcal{U}_x = (\mathcal{U}_\lambda)^\dagger \circ (\mathcal{U}_\lambda \circ \mathcal{U}_\lambda^\dagger)^{\dagger n} \circ (\mathcal{U}_\lambda \circ \mathcal{U}_\lambda^\dagger)^n \circ \mathcal{U}_\lambda. \quad (37)$$

In ideal case, $\lambda = 0$, $(\mathcal{U}_\lambda)^\dagger = \mathcal{U}_\lambda^\dagger = \mathcal{U}^\dagger$, we have

$$(\mathcal{U}_x)^\dagger \circ \mathcal{U}_x \Big|_{\lambda=0} = \tilde{\mathcal{U}}_{2x+1} \Big|_{\lambda=0}, \quad (38)$$

FIG. 3. The circuits to measure p_e of p_f and $\langle \hat{O} \rangle$ simultaneously for folding gate \mathcal{U}_n .

thus we can consider the echo instead

$$p_e(x) = \text{Tr} [\rho \rho_x], \quad (39)$$

where $\rho_x = \tilde{\mathcal{U}}_{2x+1}(\rho)$ is a physical state, to determine the error rates. For ideal state, we measure the ideal echo as $p_{e0} = \text{Tr}[\hat{P}_0 \rho] = p(\rho)$, which is the purity of initial state ρ , thus the echo is a purity-like quantity.

The echo given above is coincident with the purity if the error channels satisfy

$$(\mathcal{E}_1)^\dagger = \mathcal{E}_2, \quad (40)$$

which is not satisfied in general case. However, the advantage is that the echo is easier to measure than purity. Since the initial state can usually reduce to a pure state, and typically, $|0\rangle$, the echo is the recurrence probability

$$p_e(x) = \text{Tr} [\hat{P}_0 \rho_x], \quad (41)$$

which can be measured from projective measurement. If we want to measure the echo and the observable expectations simultaneously, we can use the nondestructive measurement, like Hadamard test or phase estimation. In conclusion, to measure the echo, we need not the copy of system, and the complicated circuit of $\hat{S}^{(M)}$. In the contrary, we lose the universality, as well as, the accuracy to some extent.

As the method described above, we measure the curve of $p = p(x)$ or $p = p_e(x)$ to determine the error rate x , which is used to extrapolate the expectation $O(x)$. For echo, the inverse function $x = p_e^{-1}(p_e)$ exists in the neighborhood of the zero $x = 0$, then the expectation $O(x)$ can locally be written as the function of echo p_e

$$O(p_e) = O[p_e^{-1}(p_e)]. \quad (42)$$

Then, we consider another quantity

$$\begin{aligned} p_f(x) &= p_e(x/2) = \text{Tr} [\hat{P}_0 \tilde{\mathcal{U}}_{x+1}(\rho)] \\ &= \text{Tr} [\rho_0 \mathcal{E}_b \circ \mathcal{E}_x(\rho_0)] \\ &\xrightarrow{x \gg 1} \text{Tr} [\rho_0 \mathcal{E}_x(\rho_0)] = \text{Tr} [\rho_0 \rho(x)]. \end{aligned} \quad (43)$$

When x is large enough, the impact of error channel \mathcal{E}_b in the last can be ignored, so this quantity approximates to the fidelity of noisy state $\rho(x)$ with the ideal state ρ_0 , which is a pure state. With this quantity, we can get the error rate near $x = 0$ locally as

$$x = p_f^{-1}(p_f) = 2p_e^{-1}(p_f). \quad (44)$$

Assume the quantity of ideal state $p_{e0} = \text{Tr}[\hat{P}_0 \rho]$ is measured same as the case of echo, then the ideal error rate is

$$x_0 = p_e^{-1}(p_{e0}) = \frac{1}{2} p_f^{-1}(p_{e0}). \quad (45)$$

So, the expectation

$$O(p_f) = O[p_f^{-1}(p_f)] \quad (46)$$

is extrapolated to

$$p_{f0} = p_f \left(\frac{1}{2} p_f^{-1}(p_{e0}) \right) \quad (47)$$

The reason we use the quantity $p_f(x)$ is that for the folding gate with odd $m = 2n + 1$ layers, the depth of circuit to measure the p_e is $2m$ layer, while p_f with $m + 1$. Therefore, the time complexity of quantum circuits measuring p_f is less than p_e . The circuits are shown in Fig. 3.

D. Efficiency

In this subsection, we consider the overhead [9, 17] of extrapolation assisted with purity. The overhead actually depends on the fitting model used. Here, we do not assume any specific fitting model, but an abstract one

$$O_{em} = O(0) = F(\{p_i, O_i\}), \quad (48)$$

where $\{p_i, O_i\}$ is all the data of purity and observable expectation from experiment. Then, we calculate the overhead C_{em} of extrapolation with purity.

Since the estimator O_{em} is not linear, thus the variance is not defined rigidly. But up to linear order, we can derive it approximately.

$$\text{Var}[O_{em}] \sim \text{Var}[\Delta F] \quad (49)$$

$$\begin{aligned} &= \text{Var} \left[\sum_i \left(\frac{\partial F}{\partial O_i} \Delta O_i + \frac{\partial F}{\partial p_i} \Delta p_i \right) \right] \\ &= \sum_i \left(\frac{\partial F}{\partial O_i} \right)^2 \text{Var}[O_i] + \left(\frac{\partial F}{\partial p_i} \right)^2 \text{Var}[p_i] \\ &\sim \text{Var}[O] \sum_i \left(\frac{\partial F}{\partial O_i} \right)^2 + \text{Var}[p] \sum_i \left(\frac{\partial F}{\partial p_i} \right)^2. \end{aligned} \quad (50)$$

By the law of large numbers (LLN), the overhead is

$$\begin{aligned} C_{em} &\equiv \frac{N^\epsilon(O_{em})}{N^\epsilon(O)} = \frac{\text{Var}[O_{em}]}{\text{Var}[O]} \\ &\sim \sum_i \left(\frac{\partial F}{\partial O_i} \right)^2 + \frac{\text{Var}[p]}{\text{Var}[O]} \sum_i \left(\frac{\partial F}{\partial p_i} \right)^2 \\ &\sim C_{em}^{\text{ZNE}} + \frac{\text{Var}[p]}{\text{Var}[O]} \sum_i \left(\frac{\partial F}{\partial p_i} \right)^2, \end{aligned} \quad (51)$$

where $N^\epsilon(O_{em})$ and $N^\epsilon(O)$ is the number of shots to measure the mitigated estimator O_{em} and the raw estimator O up to ϵ precision correspondingly. Here, we assume the overhead of ordinary ZNE method $C_{em}^{\text{ZNE}} \sim \sum_i \left(\frac{\partial F}{\partial O_i} \right)^2$ approximates to the observable expectation part of the overhead of extrapolation with purity.

The reason is that the purity influence the mitigated estimator O_{em} via the error-rate-like index s , thus the fitting model $O(s)$ is similar to the one $O(x)$ of ZNE.

In the second term of the overhead C_{em} , the part depending on F is correlated to the specific fitting model. We only consider the variance $\text{Var}[p]$ of purity in the latter. The variance $\text{Var}[p]$ depends on the method to measure the purity, and as we previously discussed, there are two kinds of methods to measure the purity. One is the replica measurement method, which is based on the Eq. (34). Another one is the QST-like method, QST and classical shadow, which measure the expectation of all Pauli operators $\langle \hat{\sigma}_\alpha \rangle$, where $\alpha \in \{1, 2, \dots, 4^L - 1\}$, and L is the subsystem size of interest. The purity by definition is

$$p = \frac{1}{2^L} \left(1 + \sum_\alpha \langle \hat{\sigma}_\alpha \rangle^2 \right). \quad (52)$$

Then, we calculate the overhead of these two different measurement methods respectively.

For the replica measurement method, the variance of purity is

$$\text{Var}[p] = \frac{1}{N} \text{Var} \left[\hat{S}^{(2)} \right] = \frac{1 - p^2}{N}. \quad (53)$$

Next, if we assume the observable of interest is a Pauli operator, we have $\text{Var}[O] = \frac{1 - O^2}{N}$, thus

$$\frac{\text{Var}[p]}{\text{Var}[O]} = \frac{1 - p^2}{1 - O^2}. \quad (54)$$

When the error rate $x \rightarrow 1$, we have $p \rightarrow 1$, if $O \not\rightarrow 1$, then the second term of the overhead C_{em} has less influence, and we have

$$C_{em} \sim C_{em}^{\text{ZNE}}. \quad (55)$$

In the contrary, if $O \rightarrow 1$ also, with Eq. (28) and (29), we have

$$\frac{\text{Var}[p]}{\text{Var}[O]} \rightarrow \frac{1 - p}{1 - O} \rightarrow \frac{2K_A}{K_B} \equiv 2\kappa < \infty, \quad (56)$$

where $K_A \equiv \sum_a A_a(0) \Re(k_a)$, and $K_B \equiv \sum_a B_a(0) k_a = \sum_a \tilde{B}_a(0) \Re(k_a)$. The second equality of K_B is because that $O = \langle \hat{O} \rangle$ is real. Then the overhead is

$$C_{em}^{\text{ZNE}} \lesssim C_{em} \lesssim C_{em}^{\text{ZNE}} + 2\kappa \sum_i \left(\frac{\partial F}{\partial p_i} \right)^2. \quad (57)$$

For the QST-like measurement method, we assume the observable \hat{O} is a Pauli operator located on L qubits, namely \hat{O} is not identity \hat{I} exactly on L qubits, and we call it L -weight Pauli operator in below. Then, the variance of purity of these

L qubits is

$$\begin{aligned}\text{Var}[p] &= \text{Var} \left[\sum_{\alpha} \frac{\partial p}{\partial \sigma_{\alpha}} \Delta \sigma_{\alpha} \right] = \sum_{\alpha} \left(\frac{\partial p}{\partial \sigma_{\alpha}} \right)^2 \text{Var}[\sigma_{\alpha}] \\ &= \frac{1}{4^{L-1}} \sum_{\alpha} \langle \hat{\sigma}_{\alpha} \rangle^2 \text{Var}[\sigma_{\alpha}].\end{aligned}\quad (58)$$

We measure the 3^L different L -weight Pauli operators with the same number N_L of shots to perform the QST-like method. To estimate the l -weight Pauli operator shorter than L , the measurement results of L -weight Pauli operators, which have the same components of $\{X, Y, Z\}$ on the nontrivial l qubits as l -weight operator, can be used, namely $N_l = 3^{L-l}N_L$. Thus, by LLN, the variance of l -weight Pauli operator is

$$\text{Var}[\sigma_{|\alpha|=l}] \sim \frac{N_L}{N_l} \text{Var}[\sigma_{|\alpha|=L}] = 3^{l-L} \text{Var}[O]. \quad (59)$$

Dividing the summation of α into the summation of weight $|\alpha| = l$, we have

$$\begin{aligned}\text{Var}[p] &= \frac{1}{4^{L-1}} \sum_{l>0} 3^l C_L^l \overline{\langle \hat{\sigma}_{|\alpha|=l} \rangle^2} \text{Var}[\sigma_{|\alpha|=l}] \\ &\sim \frac{\text{Var}[O]}{4^{L-1}} \sum_{l>0} 3^{2l-L} C_L^l \overline{\langle \hat{\sigma}_{|\alpha|=l} \rangle^2} \\ &\lesssim \frac{4\text{Var}[O]}{12^L} \sum_{l>0} 3^{2l} C_L^l = \frac{4(10^L - 1)}{12^L} \text{Var}[O],\end{aligned}\quad (60)$$

where $\overline{\langle \hat{\sigma}_{|\alpha|=l} \rangle^2} \equiv \frac{1}{3^l C_L^l} \sum_{|\alpha|=l} \langle \hat{\sigma}_{\alpha} \rangle^2 \leq 1$. Therefore, the overhead is bounded as

$$\tilde{C}_{em}^{\text{ZNE}} \lesssim C_{em} \lesssim \tilde{C}_{em}^{\text{ZNE}} + \frac{4(10^L - 1)}{12^L} \sum_i \left(\frac{\partial F}{\partial p_i} \right)^2. \quad (61)$$

When $L \rightarrow \infty$, the second term in the rightest inequality goes to zero, which means that the overhead

$$\lim_{L \rightarrow \infty} C_{em} \sim \tilde{C}_{em}^{\text{ZNE}}. \quad (62)$$

This result is actually of intuition, which states that the Pauli operators of higher weight have more contribution to purity [10], thus the variance of purity $\text{Var}[p]$ is well controlled by the variance of the highest weighted Pauli operator $\text{Var}[O]$. However, we note that the overhead of ZNE $\tilde{C}_{em}^{\text{ZNE}}$ here is calculated under the assumption that the expectation of $\langle \hat{O} \rangle$ is measured from QST-like method. In the ZNE method, we need not perform QST to measure $\langle \hat{O} \rangle$, thus the real ZNE overhead is

$$C_{em}^{\text{ZNE}} \sim 3^{-L} Z \tilde{C}_{em}^{\text{ZNE}}, \quad (63)$$

where Z is the number of different L -weight operators \hat{O}_i of

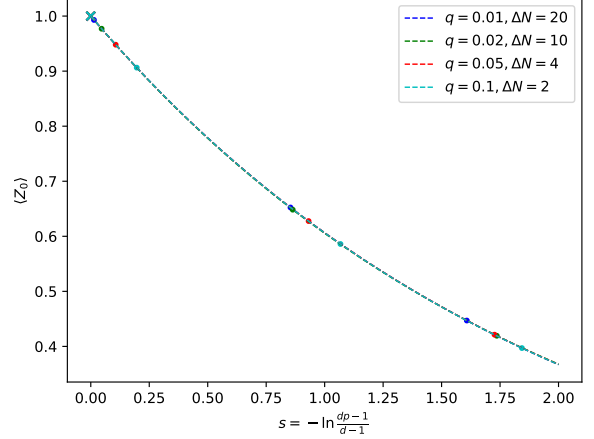


FIG. 4. Simulation result mitigated by extrapolation with purity of the expectation $\langle \hat{Z}_0 \rangle$ with the output state of CNOT gate with initial state $|00\rangle$. The fitting model is exponential model. The error model is the depolarizing error, with different error rates q . For each error rate, three instances of folding sequence are sampled for fitting, and the folded number ΔN between each sample are different for different error rates. The purity and observable are measured by QST, where each Pauli basis of 2-weight are measured with 1000 times.

interest. Therefore, the overhead asymptotically is

$$\lim_{L \rightarrow \infty} C_{em} \sim \frac{3^L}{Z} C_{em}^{\text{ZNE}}. \quad (64)$$

From this result, we find that the more the operators of interest are, and the smaller the subsystem the operators located in is, the more efficient the extrapolation with purity is.

V. SIMULATION OF EXTRAPOLATION WITH PURITY

In this section, we simulate the purity extrapolation method numerically and experimentally.

A. Numerical Simulation

First, we verify the effectiveness of purity extrapolation by numerical simulation. The CNOT gate under depolarizing error of different error rates are simulated. The initial state is selected as the $|00\rangle$ state, and the observable expectation $\langle \hat{Z}_0 \rangle$ is measured to present the effect of error. For ideal CNOT gate, the expectation $\langle \hat{Z}_0 \rangle = 1$ is invariant for any number of folding. However, the depolarizing error will lead the expectation to decay. The mitigated expectation is obtained by extrapolation with purity, which is close to the ideal expectation $\langle \hat{Z}_0 \rangle = 1$. The result is shown in Fig. 4. The decay of expectation well accords with the theoretical result of relation

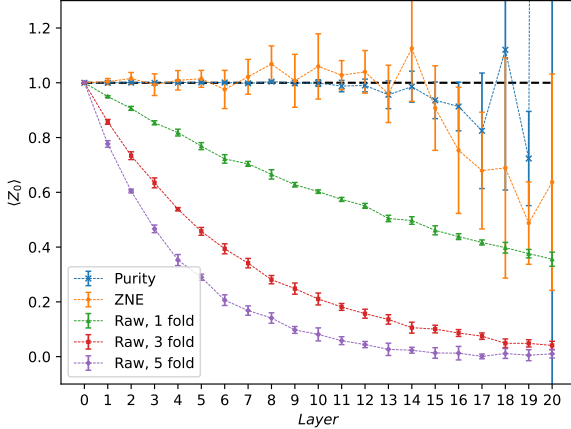


FIG. 5. The simulation results of purity extrapolation and ZNE. The CNOT-gate layers are simulated under the depolarizing error of error rate $q = 0.05$ per layer. Each circuit is simulated with 10 times, and each 2-weight Pauli basis with 1000 times measurement for QST. The raw data of expectation $\langle \hat{Z}_0 \rangle$ and the mitigated data are shown with their standard deviations.

between expectation and purity

$$\langle \hat{Z}_0 \rangle = e^{-\frac{1}{2}s} = \left(\frac{dp-1}{d-1} \right)^{\frac{1}{2}}, \quad (65)$$

which is derived from the depolarizing error model.

Then, we compare the extrapolation with purity to the original ZNE method. We still perform the CNOT gate simulated under the depolarizing error as verification. The initial state and the observable are the same with the previous one. Each layer of CNOT gate is folded, and extrapolated by purity or ZNE. We simulate the circuit with different layers, and shown the result in Fig. 5. Both the expectation and purity are measured by QST.

In the Fig. 5, the average mitigated data of extrapolation with purify and ZNE are close in the beginning. Before the 10-th layer, the average mitigated data of extrapolation with purity are closer to the ideal value than that of ZNE, and the standard deviation of extrapolation with purity are much less than ZNE. We note that this reduction of standard deviation is not majorly due to LLN. Because the total number of purity extrapolation is 3 times of ZNE, and the overhead C_{em} of purity extrapolation is larger than that of ZNE from QST \tilde{C}_{em}^{ZNE} .

Then, the precision is $\epsilon = \sqrt{\frac{\text{Var}[O_{em}]}{N}} = \sqrt{\frac{C_{em}\text{Var}[O]}{N}}$, and reduction of LLN is

$$\begin{aligned} \frac{\epsilon_{\text{pty}}}{\epsilon_{\text{ZNE}}} &= \sqrt{\frac{N_{\text{ZNE}}}{N_{\text{pty}}} \frac{C_{em}^{\text{pty}}}{\tilde{C}_{em}^{\text{ZNE}}}} \gtrsim \sqrt{\frac{N_{\text{ZNE}}}{N_{\text{pty}}}} \\ &= \frac{1}{\sqrt{3}} \approx 0.577. \end{aligned} \quad (66)$$

However, the deviation of purity extrapolation is less than

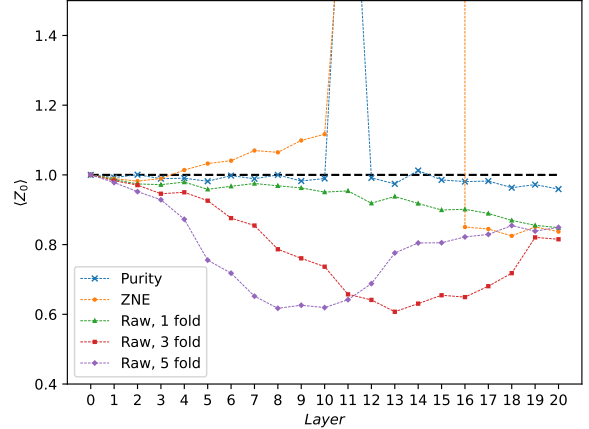


FIG. 6. The experimental results of purity extrapolation and ZNE. The expectation $\langle \hat{Z}_0 \rangle$ with the initial state $|00\rangle$ under increasing CNOT gate folding layers is shown. The fitting model is exponential model. Each Pauli basis is repeated measured with 1000 times.

ZNE an order of magnitude at least before the 10-th layers. This means that there are fluctuations other than measurement fluctuation in ZNE, which can be fixed with purity, contributing to the deviation.

After the 11-th layer, the bias between the average value of extrapolation with purity and the ideal value increases, while the standard deviations of extrapolation with purity are still much lower than that of ZNE. When after the 14-th layer, the bias and the standard deviation of extrapolation with purity and ZNE grow up rapidly. The reason is that the states of 3- and 5-folding after such large layers are close to the completely mixed state, whose expectations and purity are heavily influenced by the random fluctuation of measurement. Thus, we need more number of measurement to promote the precision. This result shows that the mitigated data of extrapolation with purity is better than ZNE in the low-error stage.

B. Experiment

We perform the extrapolation with purity and ZNE on the cloud-based superconducting quantum computer, *Quafu* [42]. The setting of experiment is same as the case of the numerical simulation, but is performed only once. The result is shown in Fig. 6. However, different with the simulation, where only depolarizing error is under consideration, the raw date of observable expectation $\langle \hat{Z}_0 \rangle$ and purity are not monotonically decreasing with the layer increasing. This lead to the undesired behavior of ZNE at the stage where the number of layers larger than 10. With the help of purity, the mitigated data of extrapolation with purity is closer to the ideal expectation $\langle \hat{Z}_0 \rangle = 1$, except at the 11-th layer, where the expectation of 3- and 5-foldings are cross. This result shows the advantage of using error witness, like purity, to assist the extrapolation that the extrapolation with purity is more stable under differ-

ent kinds of noise than ZNE.

VI. CONCLUSION

In this paper, we discuss the method using purity to determine the error rates of noise, which is in principle more accurate than the conventionally presumed error rates in the ZNE method. With purity, we can perform the ZNE method without the inaccuracy of error rates for the different error models of noise. Thus, this method can make sure the accuracy and the universality in principle. Besides, we describe the fitting model of the observable expectation versus error rate as quasi-polynomial, which is derived from the linearity of quantum system.

We calculate the overhead of the extrapolation with purity under different methods of purity estimation, the replica measurement method and the QST-like method. We show that for both estimation method the overhead of the extrapolation with purity is larger than ZNE method, while the upper bounds behave differently. The overhead of replica measurement method is bounded by the overhead of ZNE adding a finite constant, while the overhead of QST-like method will increase exponentially with the increasing of subsystem size of interest.

For the exponentially increasing overhead, the extrapolation with purity is not efficient for large system via QST-like method. However, the complexity of the quantum circuit of the replica measurement method also limits its implementation. Thus, the variational method based on the echo or state

verification method are proposed. This method has a simpler quantum circuit than the replica measurement method, but its universality and accuracy will be lost to some extent.

We have verified the purity extrapolation method with the numerical simulations under depolarizing error and the experiments on the quantum computer, *Quafu*. It has been compared with the conventional method of ZNE. The result shows that purity extrapolation can perform better than ZNE when the error rate is moderate. The standard deviation of purify extrapolation is lower than ZNE, which seems to imply that purity extrapolation is more stable under the random fluctuation of measurement at low-error stage. It has also shown that the extrapolation assisted with error witness, like purity, is more stable than the extrapolation with presumed error rate under different kinds of error.

Our results demonstrate that purity of the noisy state can be used in the ZNE method to evaluate the volume of noise. We expect that it will reinforce the wide usage of the ZNE method in NISQ era.

ACKNOWLEDGMENTS

This work was supported by National Natural Science Foundation of China (Grants Nos.92265207, T2121001, 11934018, 12122504), Innovation Program for Quantum Science and Technology (Grant No. 2021ZD0301800), Beijing Natural Science Foundation (Grant No. Z200009), and Scientific Instrument Developing Project of Chinese Academy of Sciences (Grant No. YJKYYQ20200041).

[1] B. M. Terhal, Quantum error correction for quantum memories, *Rev. Mod. Phys.* **87**, 307 (2015).

[2] E. Knill, R. Laflamme, and W. Zurek, Threshold accuracy for quantum computation, [arXiv:9610011](https://arxiv.org/abs/9610011) (1996).

[3] D. Aharonov and M. Ben-Or, Fault-tolerant quantum computation with constant error, in *Proceedings of the Twenty-Ninth Annual ACM Symposium on Theory of Computing*, STOC '97 (Association for Computing Machinery, New York, NY, USA, 1997) p. 176–188.

[4] A. Y. Kitaev, Quantum computations: algorithms and error correction, *Russian Mathematical Surveys* **52**, 1191 (1997).

[5] Y. Zhao, Y. Ye, H.-L. Huang, Y. Zhang, D. Wu, H. Guan, Q. Zhu, Z. Wei, T. He, S. Cao, *et al.*, Realization of an error-correcting surface code with superconducting qubits, *Phys. Rev. Lett.* **129**, 030501 (2022).

[6] G. Q. Ai, Suppressing quantum errors by scaling a surface code logical qubit, *Nature* **614**, 676 (2023).

[7] J. Preskill, Quantum Computing in the NISQ era and beyond, *Quantum* **2**, 79 (2018).

[8] S. Endo, Z. Cai, S. C. Benjamin, and X. Yuan, Hybrid quantum-classical algorithms and quantum error mitigation, *Journal of the Physical Society of Japan* **90**, 032001 (2021).

[9] Z. Cai, R. Babbush, S. C. Benjamin, S. Endo, W. J. Huggins, Y. Li, J. R. McClean, and T. E. O'Brien, Quantum error mitigation, [arXiv:2210.00921](https://arxiv.org/abs/2210.00921) (2023).

[10] Y. Quek, D. S. França, S. Khatri, J. J. Meyer, and J. Eisert, Exponentially tighter bounds on limitations of quantum error mitigation, [arXiv:2210.11505](https://arxiv.org/abs/2210.11505) (2023).

[11] Y. Li and S. C. Benjamin, Efficient variational quantum simulator incorporating active error minimization, *Phys. Rev. X* **7**, 021050 (2017).

[12] K. Temme, S. Bravyi, and J. M. Gambetta, Error mitigation for short-depth quantum circuits, *Phys. Rev. Lett.* **119**, 180509 (2017).

[13] S. Endo, S. C. Benjamin, and Y. Li, Practical quantum error mitigation for near-future applications, *Phys. Rev. X* **8**, 031027 (2018).

[14] Z. Cai, Multi-exponential error extrapolation and combining error mitigation techniques for nisq applications, *npj Quantum Information* **7**, 80 (2021).

[15] X. Bonet-Monroig, R. Sagastizabal, M. Singh, and T. E. O'Brien, Low-cost error mitigation by symmetry verification, *Phys. Rev. A* **98**, 062339 (2018).

[16] S. McArdle, X. Yuan, and S. Benjamin, Error-mitigated digital quantum simulation, *Phys. Rev. Lett.* **122**, 180501 (2019).

[17] Z. Cai, A practical framework for quantum error mitigation, [arXiv:2110.05389](https://arxiv.org/abs/2110.05389) (2021).

[18] B. Koczor, Exponential error suppression for near-term quantum devices, *Phys. Rev. X* **11**, 031057 (2021).

[19] W. J. Huggins, S. McArdle, T. E. O'Brien, J. Lee, N. C. Rubin, S. Boixo, K. B. Whaley, R. Babbush, and J. R. McClean, Virtual distillation for quantum error mitigation, *Phys. Rev. X* **11**, 041036 (2021).

[20] M. Huo and Y. Li, Dual-state purification for practical quantum error mitigation, *Phys. Rev. A* **105**, 022427 (2022).

[21] Z. Cai, Resource-efficient purification-based quantum error mitigation, [arXiv:2107.07279](https://arxiv.org/abs/2107.07279) (2021).

[22] J. R. McClean, M. E. Kimchi-Schwartz, J. Carter, and W. A. de Jong, Hybrid quantum-classical hierarchy for mitigation of decoherence and determination of excited states, *Phys. Rev. A* **95**, 042308 (2017).

[23] A. Kandala, K. Temme, A. D. Córcoles, A. Mezzacapo, J. M. Chow, and J. M. Gambetta, Error mitigation extends the computational reach of a noisy quantum processor, *Nature* **567**, 491 (2019).

[24] E. F. Dumitrescu, A. J. McCaskey, G. Hagen, G. R. Jansen, T. D. Morris, T. Papenbrock, R. C. Pooser, D. J. Dean, and P. Lougovski, Cloud quantum computing of an atomic nucleus, *Phys. Rev. Lett.* **120**, 210501 (2018).

[25] Y. Kim, C. J. Wood, T. J. Yoder, S. T. Merkel, J. M. Gambetta, K. Temme, and A. Kandala, Scalable error mitigation for noisy quantum circuits produces competitive expectation values, *Nature Physics* , 1 (2023).

[26] M. Foss-Feig, S. Ragole, A. Potter, J. Dreiling, C. Figgatt, J. Gaebler, A. Hall, S. Moses, J. Pino, B. Spaun, B. Neyenhuis, and D. Hayes, Entanglement from tensor networks on a trapped-ion quantum computer, *Phys. Rev. Lett.* **128**, 150504 (2022).

[27] C. Song, J. Cui, H. Wang, J. Hao, H. Feng, and Y. Li, Quantum computation with universal error mitigation on a superconducting quantum processor, *Science advances* **5**, eaaw5686 (2019).

[28] E. van den Berg, Z. K. Minev, A. Kandala, and K. Temme, Probabilistic error cancellation with sparse pauli-lindblad models on noisy quantum processors, [arXiv:2201.09866](https://arxiv.org/abs/2201.09866) (2022).

[29] S. Zhang, Y. Lu, K. Zhang, W. Chen, Y. Li, J.-N. Zhang, and K. Kim, Error-mitigated quantum gates exceeding physical fidelities in a trapped-ion system, *Nature communications* **11**, 587 (2020).

[30] R. Sagastizabal, X. Bonet-Monroig, M. Singh, M. A. Rol, C. Bultink, X. Fu, C. Price, V. Ostroukh, N. Muthusubramanian, A. Bruno, *et al.*, Experimental error mitigation via symmetry verification in a variational quantum eigensolver, *Phys. Rev. A* **100**, 010302 (2019).

[31] D. Zhu, S. Johri, N. M. Linke, K. A. Landsman, C. H. Alderete, N. H. Nguyen, A. Y. Matsuura, T. H. Hsieh, and C. Monroe, Generation of thermofield double states and critical ground states with a quantum computer, *Proceedings of the National Academy of Sciences* **117**, 25402 (2020).

[32] J. I. Colless, V. V. Ramasesh, D. Dahmen, M. S. Blok, M. E. Kimchi-Schwartz, J. R. McClean, J. Carter, W. A. de Jong, and I. Siddiqi, Computation of molecular spectra on a quantum processor with an error-resilient algorithm, *Phys. Rev. X* **8**, 011021 (2018).

[33] G. A. Quantum, Collaborators*†, F. Arute, K. Arya, R. Babbush, D. Bacon, J. C. Bardin, R. Barends, S. Boixo, M. Broughton, B. B. Buckley, *et al.*, Hartree-fock on a superconducting qubit quantum computer, *Science* **369**, 1084 (2020).

[34] F. Arute, K. Arya, R. Babbush, D. Bacon, J. C. Bardin, R. Barends, A. Bengtsson, S. Boixo, M. Broughton, B. B. Buckley, *et al.*, Observation of separated dynamics of charge and spin in the fermi-hubbard model, [arXiv:2010.07965](https://arxiv.org/abs/2010.07965) (2020).

[35] S. Stanisic, J. L. Bosse, F. M. Gambetta, R. A. Santos, W. Mruczkiewicz, T. E. O'Brien, E. Ostby, and A. Montanaro, Observing ground-state properties of the fermi-hubbard model using a scalable algorithm on a quantum computer, *Nature Communications* **13**, 5743 (2022).

[36] E. Van Den Berg, Z. K. Minev, A. Kandala, and K. Temme, Probabilistic error cancellation with sparse pauli-lindblad models on noisy quantum processors, *Nature Physics* , 1 (2023).

[37] Z. Cai, Quantum error mitigation using symmetry expansion, *Quantum* **5**, 548 (2021).

[38] Y. Kim, A. Eddins, S. Anand, K. X. Wei, E. Van Den Berg, S. Rosenblatt, H. Nayfeh, Y. Wu, M. Zaletel, K. Temme, *et al.*, Evidence for the utility of quantum computing before fault tolerance, *Nature* **618**, 500 (2023).

[39] T. Giurgica-Tiron, Y. Hindy, R. LaRose, A. Mari, and W. J. Zeng, Digital zero noise extrapolation for quantum error mitigation, in *2020 IEEE International Conference on Quantum Computing and Engineering (QCE)* (2020) pp. 306–316.

[40] A. Gilchrist, D. R. Terno, and C. J. Wood, Vectorization of quantum operations and its use, [arXiv:0911.2539](https://arxiv.org/abs/0911.2539) (2011).

[41] H.-Y. Huang, R. Kueng, and J. Preskill, Predicting many properties of a quantum system from very few measurements, *Nature Physics* **16**, 1050 (2020).

[42] C.-T. Chen, Y.-H. Shi, Z. Xiang, Z.-A. Wang, T.-M. Li, H.-Y. Sun, T.-S. He, X. Song, S. Zhao, D. Zheng, *et al.*, Scq cloud quantum computation for generating greenberger-horne-zeilinger states of up to 10 qubits, *Sci. China-Phys. Mech. Astron.* **65**, 110362 (2022).